Chapter

Biological Propulsion Systems for Ships and Underwater Vehicles

Naga Praveen Babu Mannam and P. Krishnankutty

Abstract

Regulations and performance requirements related to technology development on all modes of transport vehicles for reduced pollution and environmental impact have become more stringent. Greening of transport system has been recognized as an important factor concerning global warming and climate change. Thus environment-friendly technical solutions offering a reduction of noxious exhaust gases are in demand. Aquatic animals have good swimming and maneuvering capabilities and these observations have motivated research on fish-like propulsion for marine vehicles. The fish fin movements, used by fish for their locomotion and positioning, are being replicated by researchers as flapping foils to mimic the biological system. Studies show that flapping foil propulsion systems are generally more efficient than a conventional screw propeller, which suffers efficiency losses due to wake. The flapping foil propulsors usually do not cavitate and have less wake velocity variation. These aspects result in the reduction of noise and vibration. The present study will cover an overview of aquatic propulsion systems, numerical simulations of flapping foils and ship model self-propulsion experiments performed using flapping foil system, particle image velocimetry (PIV), and digital fluoroscopy studies conducted on fish locomotion. Studies performed on underwater and surface vehicles fitted with flapping fins will also be presented.

Keywords: bioinspired propulsors, digital fluoroscopy and particle image velocimetry (PIV), fish with caudal fin and pectoral fins, ships and underwater vehicles, propulsive efficiency

1. Introduction

Biological locomotion is defined as the movement of animals from one place to another place with the use of its whole body or appendages. The modes of locomotion existing in nature are classified as self-propelled, e.g., swimming (fish, shark, whale, seal, and dolphin), running (cheetah, wolf, and zebra), flying (swallow, hawk, owl, crow, and bat), jumping, slither (snakes and other reptiles), hopping (kangaroo, rabbit, and grasshopper) and gliding (flying squirrel) are mentioned in **Table 1**. This is termed as active locomotion, where it uses its own body muscles or legs for locomotion. Passive locomotion is defined as animal species that depend on the environment for transportation, e.g., beetles and spiders. The entire biological locomotion is classified into four types—aquatic locomotion (underwater or surface swimming organisms), terrestrial locomotion (moving on the ground or any other surface, tree-dwelling), fossorial locomotion (underground) and aerial locomotion

(birds flying in the air). These animals use water and air as its medium for its locomotion. Flying fish and diving birds use the air-water medium for its locomotion. The classification of biological locomotion in nature is shown in **Figure 1**. The

Active locomotion				Passive locomotion
Fossorial locomotion	**Terrestrial locomotion**	**Aquatic locomotion**	**Aerial and arboreal locomotion**	
Earthworms, golden mole, marsupial mole, ground squirrels.	Walking and running: ostrich, emu, humans. Hopping or jumping: kangaroo, rabbit, hare, jerboa. Crawling or slithering: snakes, sand snakes.	Hydraulic propulsion: jelly fish. Waterjet propulsion: ocean squids. Fish: sharks, eels, tunas. Dual medium animals: fish: eels, flying fish. Other marine mammals: whales and birds: ducks, swans, ostriches.	Active flight: insects, birds, bats, pterosaurs. Gliding: flying snake, flying squirrel, flying frog, flying fish. Soaring: vultures, eagles, gulls. Ballooning: spiders. Arboreal locomotion: brachiating gibbon.	Hydrozoans, arachnids, insects, crustaceans, remoras, angler fish, parasites.

Table 1.
Locomotion in nature.

(a)

(b)

(c)

(d)
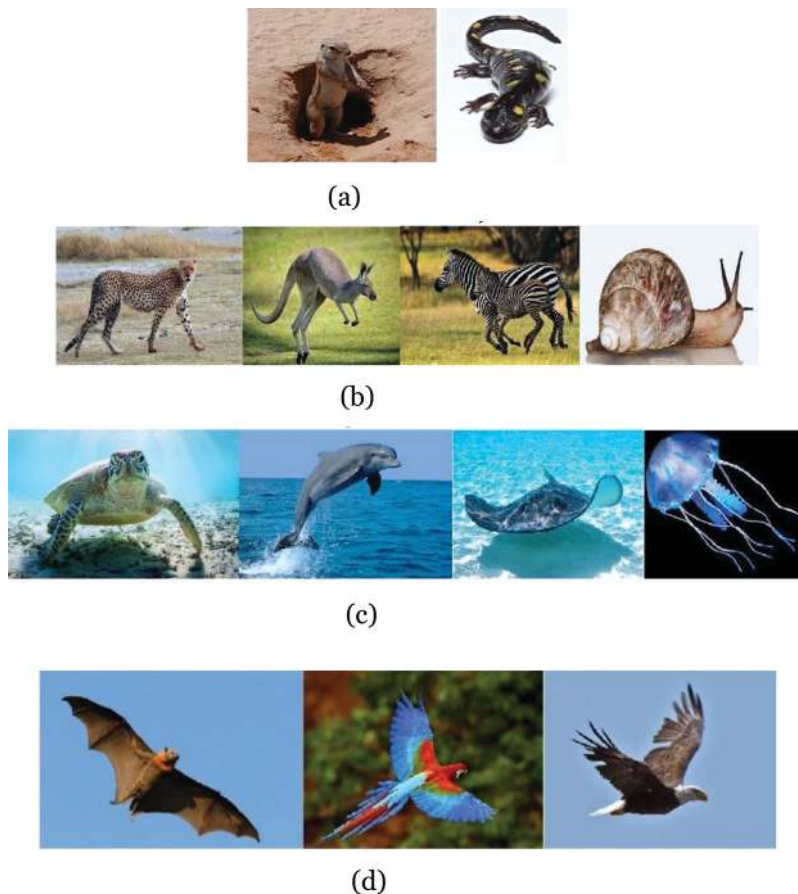
Figure 1.
Locomotion in nature. (a) Fossorial locomotion (underground) (e.g., Cape ground squirrel and mole salamanders). (b) Terrestrial locomotion—walking, hopping, running, crawling (e.g., cheetah, kangaroo, zebra, and snails). (c) Aquatic locomotion—lift based, undulation (body-caudal fin and median-paired fin modes), jet mode propulsion (e.g., turtles, dolphins, rays, and jellyfish). (d) Aerial locomotion—lift-based propulsion (e.g., bats, parrots, and eagles).
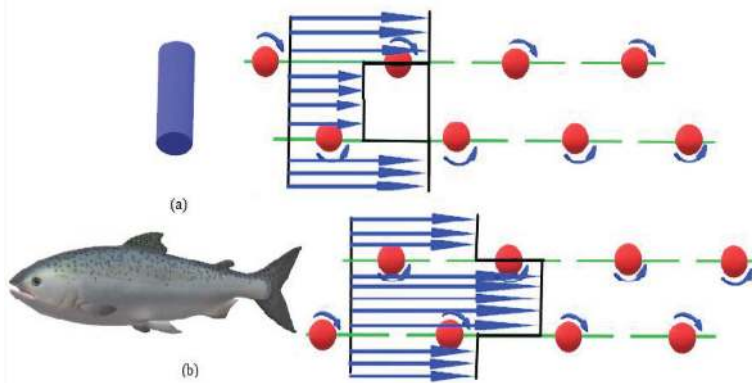
Figure 2.
(a) von Karman vortex street behind a cylinder and (b) reverse von Karman vortex street during fish swimming.

use of fossorial and terrestrial-inspired biorobots is currently used in the exploration of Martian atmospheres, robots in various defense sectors, etc. The aquatic loco-motion is currently used in designed and development of autonomous surface ships and underwater vehicles for deep-sea exploration. The aerial locomotion is used for developing flapping micro aerial vehicles and reduction of noise vibrations from wind turbine applications.
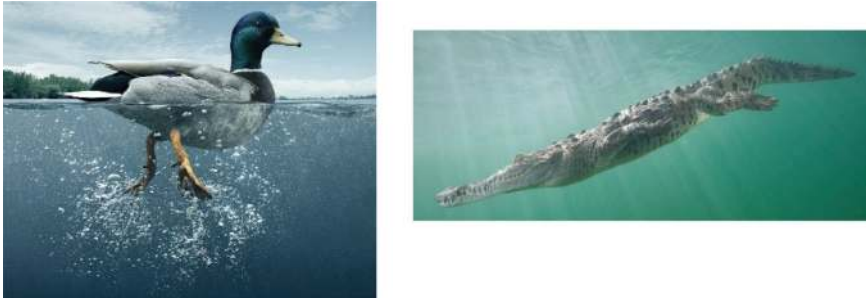
1.1 Lift-based propulsion

In lift-based propulsion, flapping foils or wings are used to create lift and hori-zontal thrust force by moving through water. It creates a pressure difference between the top and bottom surfaces of the flapping wing. The sea turtles and penguins use their paired wings for creating lift and thrust force. Mainly, lift-based propulsors are vortex enhanced propulsors. They use this vortex enhancing mecha-nism of converting von Karman vortex street to reverse von Karman vortex street. All the lift-based animals produce drag at low Strouhal numbers. These animals sense the opposing fluid force on the body and increase the frequency and ampli-tude of fins, thereby increasing the Strouhal number that is in the range of 0.2–0.5. The von Karman vortex street and reverse von Karman vortex street are shown in **Figure 2**.

1.2 Drag-based propulsion

The drag-based animals such as ducks, Nile crocodiles, frogs, and other diving animals uses cyclic motion where they push water back in power stroke and return their limbs forward, which is defined as recovery stroke (**Figure 3**). In power stroke, the animals move their body forward by using its power stroke. In return stroke, the animals move their limbs to start position by pushing water forward minimally, which results in moving the body of the animal slightly backward. During the return stroke, the swimming movement of the animal is opposed and the opposing force is known as drag. This type of propulsion for conventional vehicles results in low efficiencies.

1.3 Undulatory propulsors

In undulation mode, aquatic animals swim through the water by the creation of undulations or flag movements with their bodies or using fins. The undulation

Figure 3.
Drag-based propulsion (e.g., ducks and Nile crocodile).

mode is classified as a body-caudal fin (BCF) propulsion and median-paired fin (MPF) propulsion. The BCF mode is again subdivided into (a) anguilliform, (b) carcharhiniform (c) sub-carangiform (d) carangiform, (e) thunniform (f) esociform fish and (g) ostraciiform modes. The anguilliform and ostraciiform modes are slow swimmers and carangiform, thunniforms are relatively fast swimmers. In the anguilliform mode, slender body fish such as sea snakes, eels generate propulsive wave starting from head portion of the body to the tail portion. The sub-carangiform and carangiform group increase its wave amplitude from the middle portion of the body to rear part of the fish body. The thunniform mode of fish is high-speed long-distance swimmers. The ostraciiform group of fish is box-shaped bodies with caudal fin. Only the caudal fin itself oscillates to generate thrust. Similarly, MPF mode is classified as (a) tetraodoniform, (b) balistiform, (c) diodontiform, (d) rajiform, (e) amiiform, (f) gymnotiform and (g) labriform. In MPF mode, most of the fish use a pair of pectoral fins, anal fins or a combination of both for generating a propulsive force. The detailed classification is given in **Table 2**.

1.4 Jet propulsors

In Jet propulsion mode, aquatic animals fill their cavity by compressing the fluid and eject the fluid out to propel themselves in the opposite direction of the ejected fluid. In jet propulsion mode, the propulsion mechanisms are different from one animal to another animal. In jellyfish, it draws water from the rear and ejects it through the rear part. In scallops, fluid enters from its front portion and ejects out at its rear portion of the body.

1.5 Literature review: state of the art

Experimental and numerical methods are the oldest and most reliable sources of information on any physical studies and some do apply for the present studies on marine vehicle propulsion. The experimental studies are carried out on flapping foil propulsor by considering the effects of variations on the Strouhal number and maximum angle of attack on the thrust force which results in increasing hydrodynamic efficiency of flapping foil [1]. The pectoral fin model of bluegill sunfish is studied during its maneuvering to avoid the obstacles. This study involves biological studies of pectoral fins of sunfish, developing kinematic models of the motion of pectoral fins, 3D computational studies of pectoral fins flow characteristics and forces, and implementation of simplified models of pectoral fin kinematics and mechanical properties in a physical model [2]. The mechanical design of fish fin

Body and caudal fin (BCF) propulsion	Median and paired fin (MPF) propulsion
Anguilliform: eel	Tetraodoniform: ocean sunfish
Carcharhiniform: hammerhead sharks	Balistiform: trigger fish
Subcarangiform: rainbow trout	Diodontiform: puffer fish
Carangiform: mackerels	Rajiform: rays
Thunniform: tuna	Amiiform: bowfin fish
Esociform: northern pike	Gymnotiform: knife fish
Ostraciiform: box fish	Labriform: wrasses

Table 2.
BCF and MPF propulsors.

rays that allows active muscular control of curvature and flexibility of the fish body in propulsion are studied [3]. Experimental studies are performed on purely-pitching foil with a rigid and flexible flap of suitable stiffness. The rigid pitching foil produces a weak and meandering jet (and thrust), whereas the flexible foil produces a strong jet of the wake. Deformations of the flexible flap suppress meandering by increasing the initial gap between two successive vortices and by imposing a convective motion on the shed vortices even in the absence of free-stream velocity [4]. Four foils made of adhering layers of plastic sheets to produce discrete regions of high and low flexible stiffness of biologically-relevant magnitudes. Using a

mechanical flapping foil controller, the forces and torques in three directions (x,y,z) and the swimming performance under both heaving motion and constant 0° angles of attack case studies are carried out experimentally [5]. The 2D flapping foils in a tandem configuration in forwarding propulsion at *Re* = 5000 using experimental and numerical techniques are studied. Both tandem foils are subject to symmetrical translational and rotational motions with a Strouhal number of 0.32. The observations show that the foil-wake interaction is favorable to thrust generation, which requires the tandem wing has to cross the shear layer shed from the front wing and results in an increase in angle of attack [6]. Three-dimensional numerical simulations are carried out on tuna fish to study the flow characteristics and vorticity pattern around the fish when swimming in a straight line. The body undulation occurs at the rear half of the fish, and the caudal fin of the tuna fish oscillates with combined sway and yaw motions [7]. The underwater vehicle (UV) which has both flapping-foil and gliding function are studied. Numerical simulations are carried out in the fluent code using dynamic meshing on a single degree of freedom flapping-foil movement, which demonstrated the mechanism of flapping foil. The turbulence effects were taken into account, and the turbulent stress was evaluated by means of the realizable *k*-epsilon model [8]. The detailed hydrodynamic analysis of the thrust generated by an oscillating hydrofoil is carried out using numerical and experimental studies. The hydrofoil is mounted at the bow of a platform supply vessel as a means of auxiliary propulsion and, is vertically oscillating due to the ship's heave and pitch motions in head-waves [9]. On scrutinizing the works presented above it is clearly evident that the experimental approaches have been quite successful over years in predicting the performance of biomimetic propulsion systems for ships and AUV's. A high degree of robustness and reliability has also been observed in methods based on systems and parametric identification in the design and development of bioinspired systems for marine vehicles. Other theoretical methods can only give rough estimates of the thrust generated by flapping foils. Numerical methods Reynolds-averaged Navier-Stokes equations (RANSE)-based computational fluid dynamics (CFD) techniques have been successfully employed in simulating two-dimensional, flapping foils. The method is still in its developing stage, where a confidence level in its application to three-dimensional flapping foils problems is yet to be achieved. Many authors are currently concentrating on this research area of numerical study of 3D flapping foils for marine vehicles.

As far as the use of bioinspired propulsion systems for ocean-going vessels is concerned, the literature to date has been able to give only laboratory demonstrative models. The application of oscillating fins as propellers to conventional marine vehicles is being explored and this has given the impetus in this chapter to concentrate on bioinspired propulsion for marine vehicles. This necessitates the need for detailed experimental and numerical study on three-dimensional fish-like propulsion system used in surface and sub-surface marine vehicles. These studies are envisaged to understand the fluid particle level movements around different fish fins during a live fish swimming, mimicking these fins and its motion using the physical model in a laboratory, attach fins to surface ship and underwater vehicle models to determine the self-propulsion parameters and resulting thrust, torque and propulsive efficiency. The entire study has been divided into four sections. Section 1 gives an introduction to the study, presents the review of relevant literature and the motivation for this study. Section 2 shows the various mathematical models used for the determining hydrodynamic forces of bioinspired propulsors. Section 3 introduces examples of bioinspired propulsion systems. Section 4 summarizes the work and the conclusions from the above studies are presented.

2. Empirical methods to determine hydrodynamic forces and propulsive efficiencies of bioinspired propulsors

2.1 Estimation of propulsive forces using numerical techniques

The non-dimensional flow variables are used for the analysis of the results obtained from the numerical simulations of lift-based propulsion systems. The forces acting on flapping foil (**Figure 4a** and **b**) subjected to heaving and pitching motions are resolved in x and y-direction as $F_X(t)$ and $F_Y(t)$, respectively, and the moment about the pivot point is denoted as $M(t)$. The force coefficients are given as

$$C_X = \frac{(\overline{F}_X)}{\frac{1}{2}\,\rho\,U^2 cS} \tag{1}$$

$$C_Y = \frac{F_Y}{\frac{1}{2}\,\rho\,U^2 cS} \tag{2}$$

$$C_M = \frac{M}{\frac{1}{2}\,\rho\,U^2 c^2 S} \tag{3}$$

where U and c are the free stream velocity and hydrofoil chord length, ρ is the density of fluid respectively, and S is the span of the hydrofoil and is assumed to be unity. The thrust force created by flapping hydrofoil is $F_X(t)$. The average thrust over n complete flapping cycles over period T is given as

$$(\overline{F}_X) = \frac{1}{nT}\int\limits_{0}^{nT} F_X dt \tag{4}$$

The power required for the flapping foil, defined as the amount of energy imparted to the hydrofoil to overcome the fluid force, is given as

$$P(t) = -F_y(t)\frac{dy}{dt} - M(t)\frac{d\psi}{dt} \tag{5}$$

The sign on both the terms in Eq. (5) is negative as vertical force and moment are the reaction forces created by the fluid as the hydrofoil moves through it.

The average power over n complete cycles of flapping, over a period T, is given as

(a)   (b)
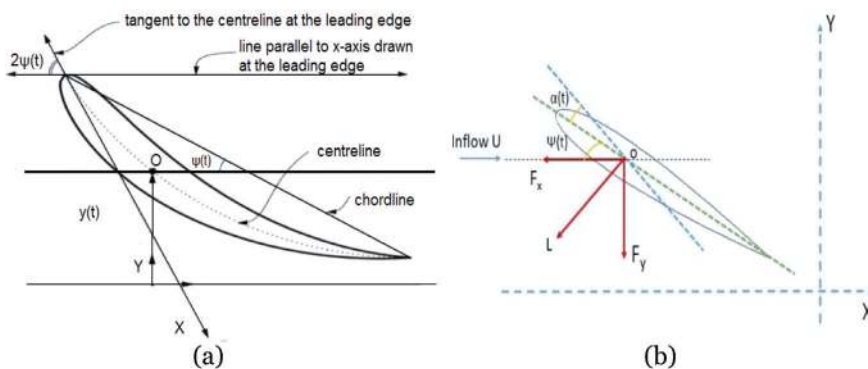
Figure 4.
Foil motion with respect to angle of attack (α), sway and yaw modes.

$$(\bar{P}) = \frac{1}{nT} \int_0^{nT} P dt \tag{6}$$

$$(P') = \frac{(\bar{P})}{\frac{1}{2} \rho U^3 cS} \tag{7}$$

The propulsive efficiency η is defined as the ratio of the output power $(\bar{F}_X)U$ to the input power $(\bar{P})$. From Eqs. (1) and (7), η is given by

$$\eta = \frac{(\bar{F}_X)U}{(\bar{P})} = \frac{(C_X)}{(P')} \tag{8}$$

2.2 Estimation of thrust and torque of pectoral fins using propeller theories

Flapping foil is composed of a series of blade elements each of which produces hydrodynamic forces such as lift, drag, thrust and torque due to the motion of the fluid. The axial component is the element thrust & the tangential component is the element torque. Integration over the radius of all sections gives total thrust & torque of the flapping foil. In this method, the pectoral flapping wing is divided into a number of independent sections along its span. At each section, a force balance is applied involving lift, drag, thrust, and torque produced by the section shown in **Figure 5**. At the same time, a balance of axial and angular momentum is also applied. This approach is applied to the flapping pectoral fins and the resulting thrust (T_h) and torque (T_q) are obtained as,

$$T_h = \int_{R_o}^{R_t} (C_L \sin \gamma - C_D \cos \gamma) \times 0.5 \times \rho \times V^2 \times C(r) dr \tag{9}$$
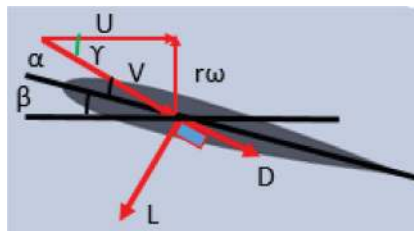
$$T_q = \int_{R_o}^{R_t} (C_L \cos \gamma + C_D \sin \gamma) \times 0.5 \times \rho \times V^2 \times C(r) r dr \tag{10}$$

Here C_L and C_D are lift coefficient and drag coefficient with a given angle of attack.
(α) and V is the velocity of flow and is given by,

$$V(r,t) = \sqrt{U^2 + (r\omega(t))^2} \tag{11}$$

The inflow angle γ is calculated as,

Figure 5.
Flapping foil blade section.

$$\gamma(r,t) = \tan^{-1}\frac{r\omega(t)}{U} \tag{12}$$

As the flapping motion is subjected to sinusoidal motion, the flapping angle $\theta(t)$ and the angular velocity $\omega(t)$ are given by the following expressions

$$\theta(t) = \theta_{max}\sin\frac{2\pi}{T}t \tag{13}$$

$$\omega(t) = \frac{2\pi}{T}\theta_{max}\cos\frac{2\pi}{T} \tag{14}$$

2.3 Estimation of torque of caudal fin

The surface ship model is fitted with caudal fin oscillation mechanism where DC servo motors are used as the prime mover. The power demand for fin oscillation depends on the fin size, its oscillation frequency, and amplitude. The stroke of the caudal fin in the x-y plane is y_G (**Figure 6**) is given by,

$$y_G = r\sin\psi \tag{15}$$

where ψ is the yaw angle. The fin is oscillating with a frequency f (Hz) and hence the instantaneous position of the fin CG is given by

$$y_G = (r\sin\psi)\sin 2\pi ft \tag{16}$$

The velocity, v_G (m/s) is given by,

$$v_G = \frac{dy_G}{dt} = 2\pi fr\sin\psi\,(\cos 2\pi ft) \tag{17}$$

when caudal fin moves to initial centerline of the fish body, $\cos 2\pi ft$ become one and hence the maximum velocity is given by,

$$v_{Gmax} = 2\pi fr\sin\psi \tag{18}$$

The maximum drag force on the caudal fin is,

$$D_{max} = C_D\left(\frac{1}{2}\right)\rho\,A_f v_{Gmax}^2 \tag{19}$$

where C_D is the drag force coefficient and A_f is the fin profile area.
The maximum torque developed by the caudal fin oscillation is,

$$Q_{max} = D_{max}r = 2\pi^2 C_D\rho\,r^3 A_f f^2 \sin^2\psi \tag{20}$$

Figure 6.
Caudal fin motion mode.

2.4 Estimation of propulsive forces from PIV experiments

In flow visualization experiments, the quantitative measures of hydrodynamic forces acting on the fish body and impulse can be determined. There are two methods for estimating the forces in a fluid, one based on the fluid momentum which is used for unsteady flows and the other one is based on fluid vorticity which is used for steady flows.

In both the cases, one first estimates impulse I, the integral of force F applied to the fluid over time, the mean force F_{mean} applied to the fluid multiplied by the total time T over which it was applied:

$$I = \int_0^T F \, dt \tag{21}$$

$$I = F_{mean} \, T \tag{22}$$

To obtain the force, differentiating I by T. Therefore,

$$F = \frac{\partial I}{\partial t} \tag{23}$$

2.4.1 Vortex analysis

The circulation is defined as the total vorticity within an area circumscribed by a closed loop. For a steadily moving vortex ring, the procedure to estimate the force generated is quite straightforward. Any sufficiently large loop that passes through the center of vortex ring has a constant circulation that is proportional to the force required to generate the ring:

$$F_{mean} = \frac{\pi \rho \Gamma D^2}{4} \tag{24}$$

where ρ is the density of the fluid, Γ is the circulation, D is the distance between the two vortex centers in the plane.

Mathematically, circulation Γ can be written in two equivalent ways:

$$\Gamma = \int_\Sigma \omega \, d\Sigma \tag{25}$$

$$\Gamma = \oint_c u \, \mathrm{dl} \tag{26}$$

where Σ is a surface in the fluid, C is the closed contour around the edge of the surface, and l is the tangent vector along the vorticity contour.

3. Examples of aquatic propulsion systems

3.1 Experimental and numerical study of a surface ship fitted with tandem flapping foils

In the present study, experimental and numerical studies are carried out to ascertain the thrust producing mechanism of flapping foils [10]. The propulsive performance of flapping foils fitted to surface ships in tandem mode at its midship

position is studied. The current work attempts to investigate the thrust generation capability and efficiency of the rigid and flexible hydrofoil in open water condition and the results of which are compared with those obtained from ship model tests in self-propulsion mode. The foil flexibility in computational fluid dynamics (CFD) environment is introduced using an appropriate user-defined function. The lift-based penguin type propulsion system installed in a ship model, used in the study, is shown in **Figure 7**. A pair of flexible flapping foils is attached to the ship model bottom. The amplitude and frequency of these flapping foil oscillations are varied using the electro-mechanical systems. In the experimental study, ship model resistance tests, bollard pull tests, and self-propulsion tests are carried out in the towing tank and the results are recorded, presented and discussed.

### 3.1.1 Flapping foil propulsion ship: resistance tests

The ship model fitted with fins and other fixtures were run in the towing tank to experimentally determine the model resistance at different speeds. The resistance force of a ship at a constant speed is the force required to tow the ship in calm water at that speed. The model is accelerated to the desired speed and the speed is kept constant. The average values of the measurements for the period of constant speed are recorded. The ship model was built in fiberglass to the scale 1:15. The towing tank dimensions are 82 m long × 3.2 m wide × 2.5 m (water depth). The model was ballasted to the loaded condition with an even keel. Model towing tests were conducted in the speed range covering the design speed. The resistance test results are shown in **Figure 8**. The effective power of the model with fins is estimated at 33.15 W at a speed of 1.2 m/s. The ship hull model (below bottom) is attached with chain sprockets, chain drives, bearing blocks, two circular shafts of 25 mm diameter to mount the flexible flapping foils stiffened with steel plates. This additional fitting attached to the ship hull caused an increase in resistance.

3.1.2 Bollard pull tests

The ship model is tied to a stationary post and the flaps oscillate at different frequencies and amplitudes corresponding to different Strouhal numbers. The thrust developed by the flapping foils is measured in each case using a load cell. The maximum thrust was found to be 21.3 N at f = 3 Hz and oscillation amplitude of 300 mm.

3.1.3 Self-propulsion tests

In self-propulsion tests, the ship model is fitted with an electric motor and load cell to measure the thrust force generated by the flapping foils. The ship speed is matched with towing carriage speed to determine the speed achieved by the ship at different frequencies and amplitudes and the forces are measured using the load cell
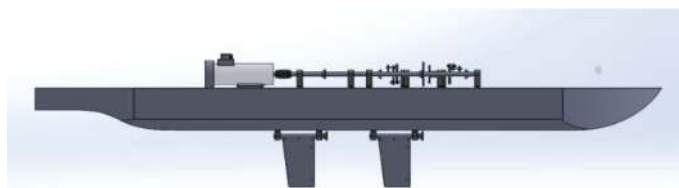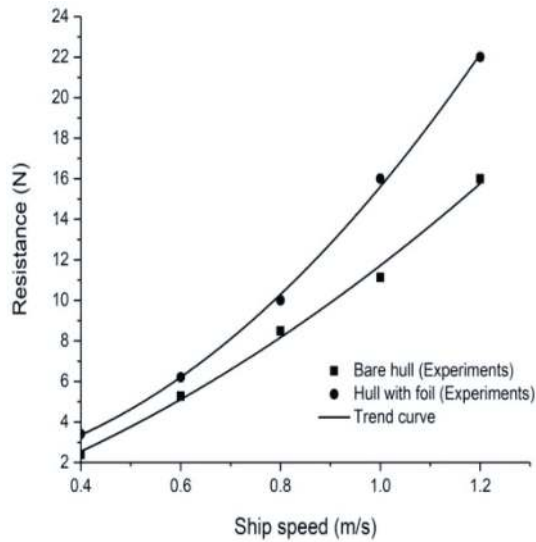

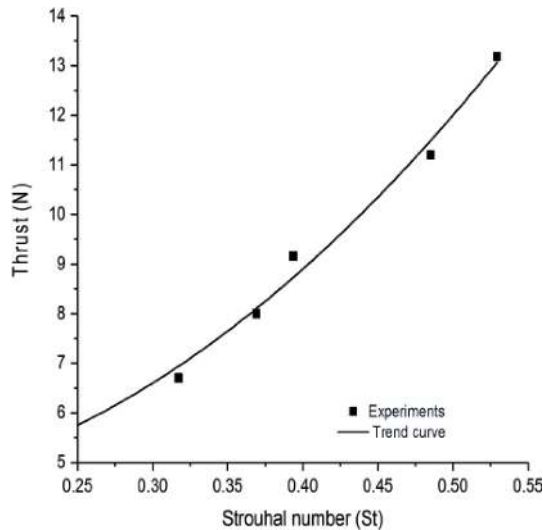**Figure 7.**
Ship model fitted with flapping foils.

and data acquisition system. The maximum thrust force of 13.18 N at St = 0.53 is measured and shown in **Figure 9**. The thrust force generated by the foils in bollard pull condition is higher when compared to the self-propulsion tests as it appears in the vessels fitted with the conventional screw propellers.

3.1.4 Numerical study of flexible and rigid flapping foil

The standard National Advisory Committee for Aeronautics airfoil section (NACA0012) with a chord length c = 0.1 m is used for the hydrofoil modeling. NACA0012 is symmetrical foil, so flap angle of attack α, is symmetrical about 0°. The NACA0012 section is mainly used for plunging and combined pitching and plunging motions in numerical simulations for fully laminar and fully turbulent flow regimes.
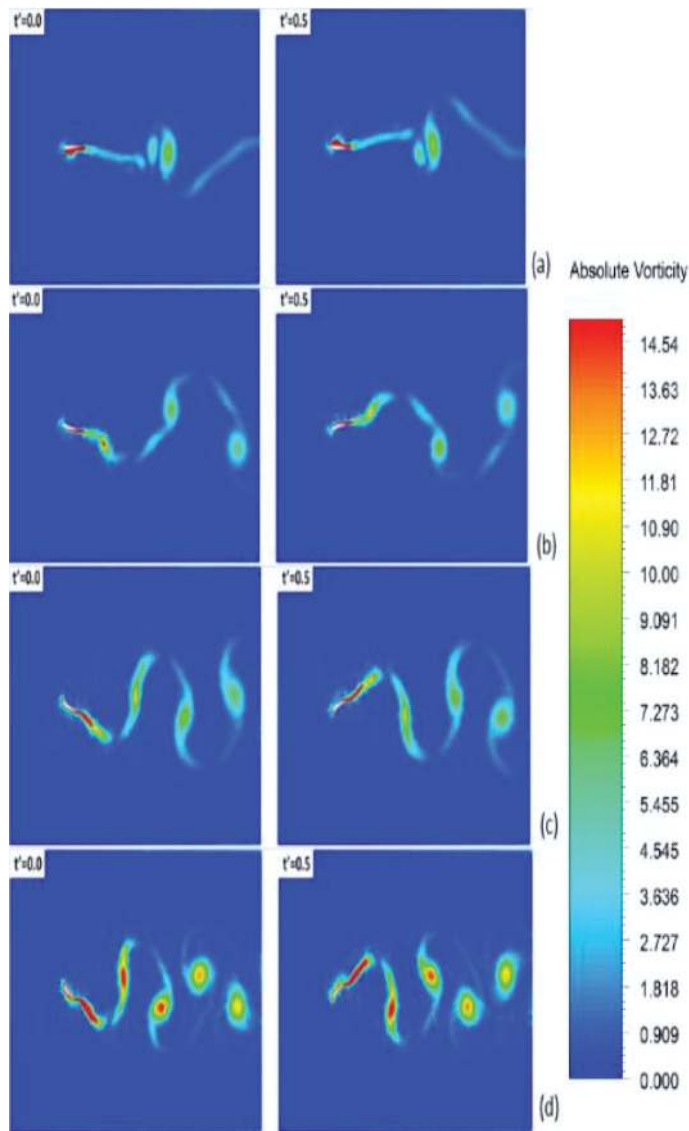

Figure 8.
Resistance tests of the ship model with and without the foils fitted.

Figure 9.
Thrust developed in self-propulsion mode ($V \neq 0$).

3.1.5 Results and discussions

The wake characteristics of rigid and flexible flapping foils are studied at different Strouhal numbers (St = 0.1–0.4) with different maximum angles of attack such as 10°, 15°, and 20°. As the flapping frequency and amplitudes are increasing (St = 0.1–0.4), the fluid flow separates from the trailing edges forms a jet of alternating vortices which results in thrust production. This formation of vortices is termed as reverse von Karman Vortices [10]. As the angle of attack increases from 10° to 20°, the vortices becomes stronger at St = 0.1 and the resulting thrust force increases. The absolute vorticity contours for flexible flapping hydrofoil at α_0 = 20° at different Strouhal numbers are shown in **Figure 10**. The variation of force and moment coefficients for flexible flapping foil is shown in **Figure 11**. The average thrust coefficient (C_X) and efficiency (η) of both rigid and flexible foils are shown
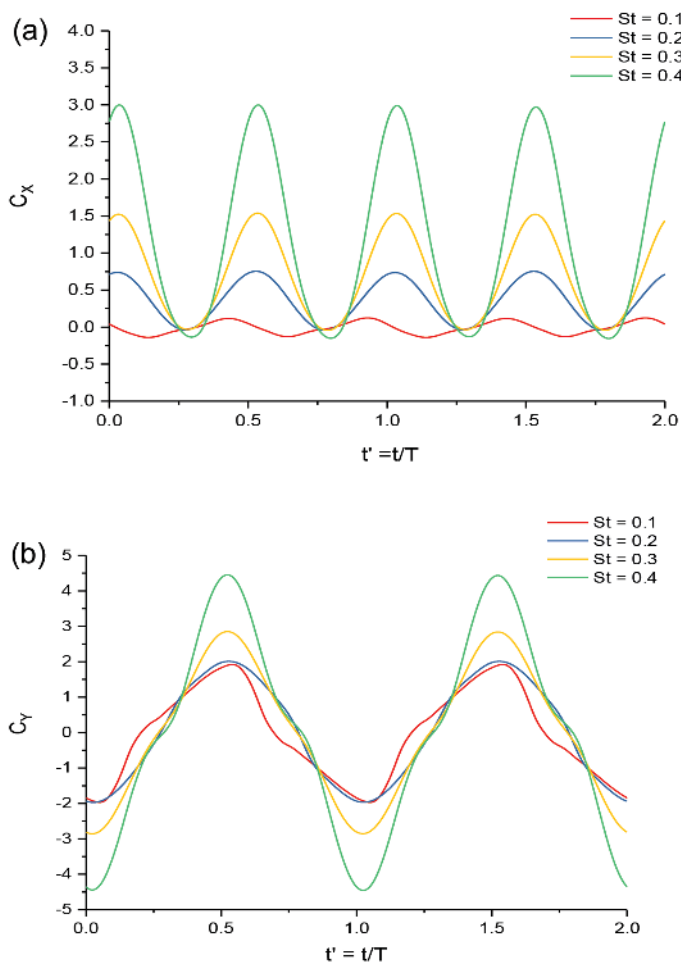

Figure 10.
Absolute vorticity contours of flexible flapping hydrofoil at α_o = 20° for (a) St = 0.1, (b) St = 0.2, (c) St = 0.3 and (d) St = 0.4.

in **Figures 12** and **13** for different angles of attack (10°, 15°, 20°). From the experimental studies in self-propulsion mode, the thrust (C_X) = 2.75 is measured at St = 0.53. In numerical studies, the maximum thrust coefficient (C_X) = 2.38 is obtained for α_0 = 20° at St = 0.55.

3.2 Obtaining 3D kinematics of fish locomotion using digital X-ray fluoroscopy

Carangiform fish play a major role in propulsion and maneuvering performance. In this section, skeletal view of the carangiform fish spine and caudal fin kinematics during forward swimming are presented using digital X-ray fluoroscopy technique. The aim of this study is to obtain the 3D kinematics of the fish spine and caudal fin motions. The X-ray recordings were possible through collaboration between the Department of Ocean Engineering, Indian Institute of Technology (IIT) Madras, India, and Sri Ramachandra Medical College (SRMC), Chennai, India. Biplanar high-speed cineradiographic fluoroscopy with an image resolution of 1536 × 1024 was taken from top view. The fish swims freely in a glass tank during the experiments. The experimental set up is shown in **Figure 14**. The spinal chord and caudal fin motions were recorded during fluoroscopy tests. These motions are tracked manually for all the videos in which fish swims straight and achieves steady state
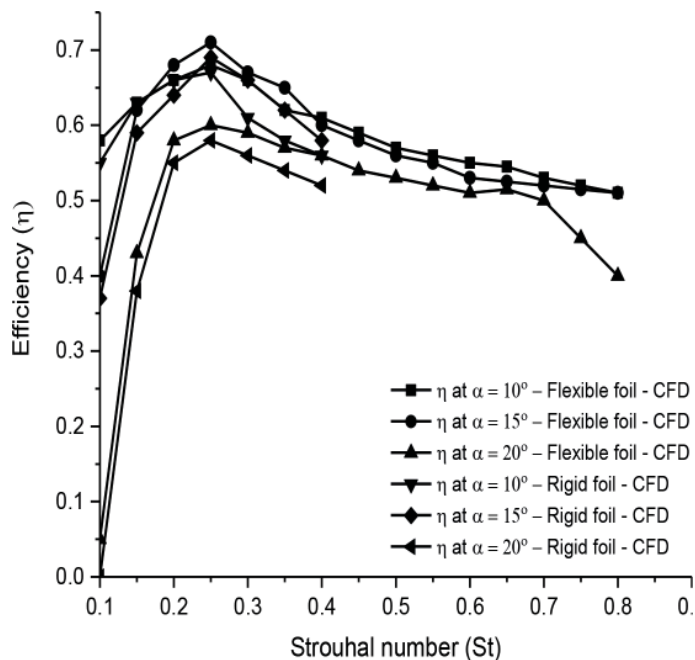

Figure 11.
Variation of (a) C_X, (b) C_Y for St = 0.1–0.4 at α_o = 20° for flexible foil.

locomotion. The fluoroscopy images of the fish spine and caudal fins are shown in **Figures 15** and **16**. As shown in **Figure 16**, the number of joints in the fish spinal chord and representation of pectoral fins, the caudal fin is marked. By using custom software, OpenCV we can track these points in the images in order to get the 3D kinematics of fish swimming which can be taken as a future study in this area.
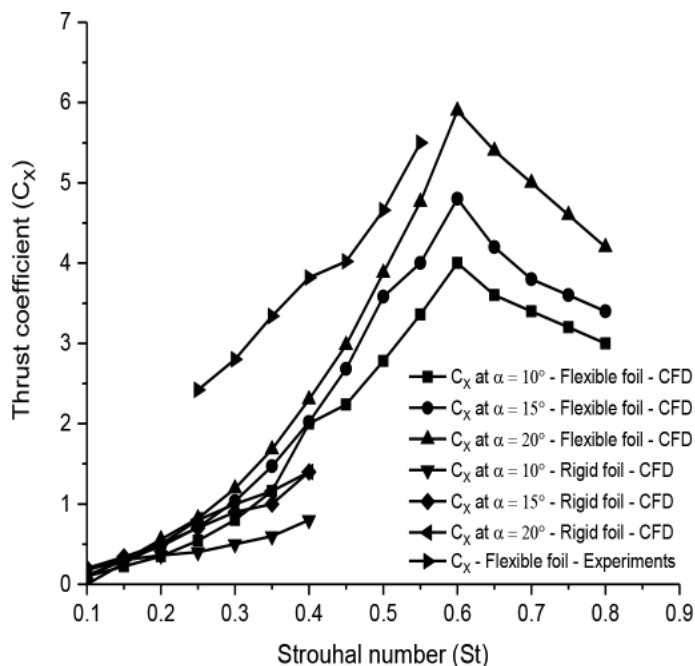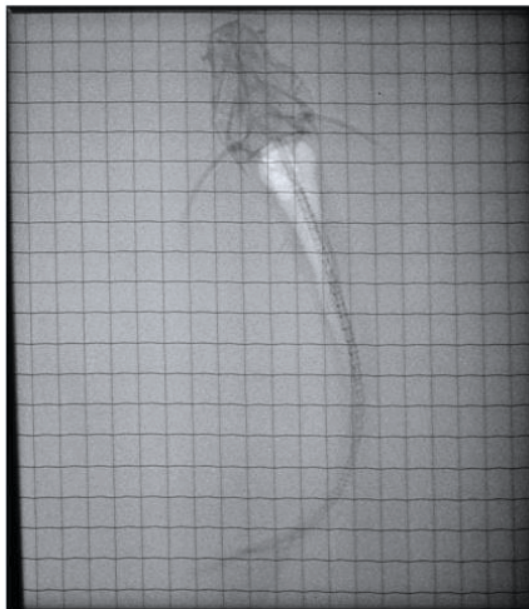
Figure 12.
Thrust coefficient at α_0 = 10°, 15° and 20° for tandem flapping foil.

Figure 13.
Propulsive efficiency at α_0 = 10°, 15° and 20° for single foil.

Figure 14.
*Digital fluoroscopy recording of fish swimming.*

Figure 15.
Fluoroscopy image of fish swimming—skeletal view.

3.3 Experimental study of fish locomotion using 2D particle image velocimetry

Two-dimensional flow visualization experiments are carried out to visualize the flow pattern around the caudal, pectoral, anal and dorsal fins of a freely swimming fish particle image velocimetry (PIV) system [11]. The freshwater black shark fish with a body length of 26 cm is used for the present experimental study. The fish is placed inside a glass tank of size $L \times B \times D = 75 \times 29 \times 37$ cm and it is allowed to swim freely in the tank shown in **Figure 17**. The PIV system used in this experiment consists of (i) a double-pulsed Nd-YAG (neodymium-doped yttrium aluminum garnet) laser with 200 mJ/pulse energy at 532 nm wavelength, (ii) a charge-coupled device (CCD) camera with a 2048×2048 pixels and an image capturing speed of 14 frames per second (fps), (iii) a set of laser and a camera controllers and, (iv) a data acquisition system. The laser sheet is aligned with the longitudinal vertical XZ and transverse YZ planes. The camera is positioned in front of the test section perpendicular to the laser sheet.
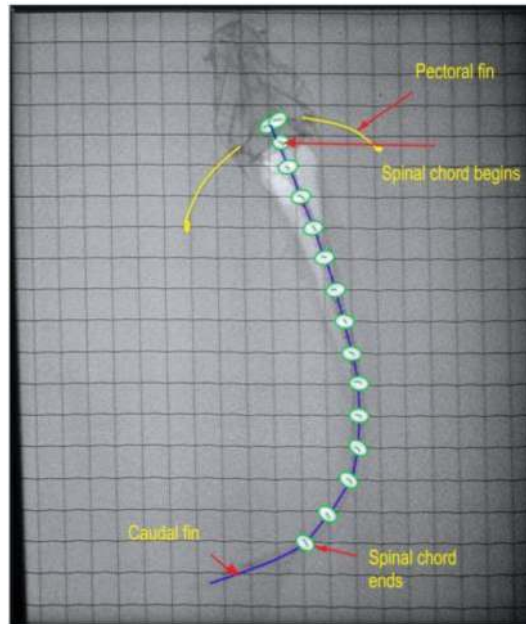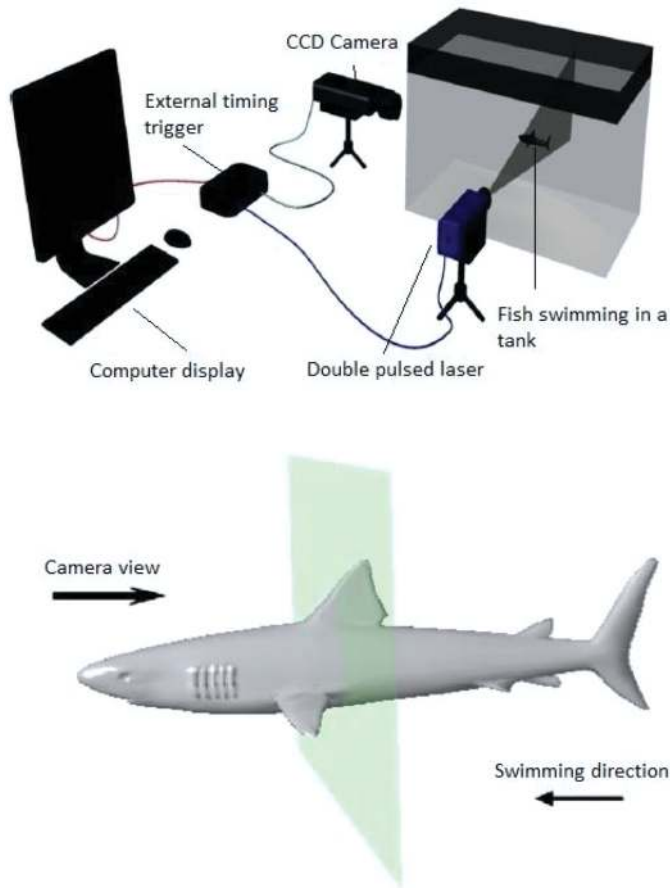
Figure 16.
Manual tracking of fish spinal chord joint and caudal fin.

Figure 17.
Freely swimming freshwater shark fish.

The PIV technique involves the introduction of tiny particles called 'seeder particles' into the fluid path. Hollow glass spheres with a mean diameter of 10 μm are used as the tracer particles. The PIV setup used in the present experiment is shown in **Figure 18**. The flows around the fins of freely swimming fish are analyzed and the velocity vector fields are presented here. In this analysis, we are presenting a raw CCD (charged coupled device) image and the processed image at different time intervals. The white boundary line represents the body contour of fish. The primary vortex regions are marked as V_1, V_2 in images. **Figure 19** shows the CCD image and velocity vector field around adipose and anal fins for $\Delta t = 900$ ms. The adipose and anal fins generated vortices, that passes downstream, interacts with caudal fin vortices which results in increasing the propulsive performance. **Figure 20** shows CCD image and velocity vector field around caudal fin stroke in YZ plane for $\Delta t = 900$ ms while the fin is at the center plane. A jet of high-velocity flow is observed at the top of the caudal fin.
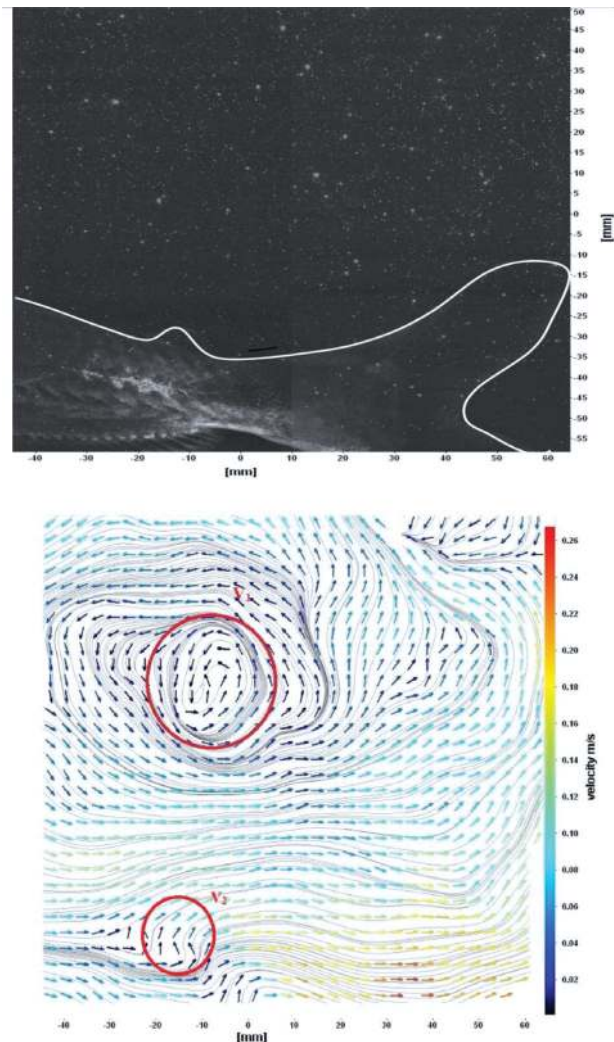
Figure 18.
PIV system arrangement.

3.4 Experimental study of a remotely operated surface ship fitted with caudal fin

The thunniform mode caudal fin propulsion system is designed and developed for a surface ship model. The caudal fin acts as a main propulsor is operated at different frequencies and amplitudes to experimentally find its propulsive performance [12]. The length of the ship model is 1.4 and 0.35 m wide. The caudal fin is actuated by single DC servo motor powered by the lithium-polyimide(lipo) battery of 25.9 V. The crank slider mechanism is used for converting the rotary motion of the motors into the fin oscillation mechanism. By coordinating the movements of the tail fin, the ship model can simulate the movements of fish in the water. **Figures 21** and **22** shows the surface ship model and caudal fin propulsion mechanism used here. The control system consists of a wireless communication unit, microprocessor, strain gauge sensors for force measurement, data acquisition system. The block diagram and tail fin motor connections are shown in **Figure 23**.

3.4.1 Results and discussions

The remotely operated surface ship model in self-propulsion mode is shown in **Figure 24**. In self-propulsion tests, the caudal fin amplitude is kept constant at 0.15 m and the frequencies are varied from 0.5 to 1.75 Hz. The caudal fin of ship
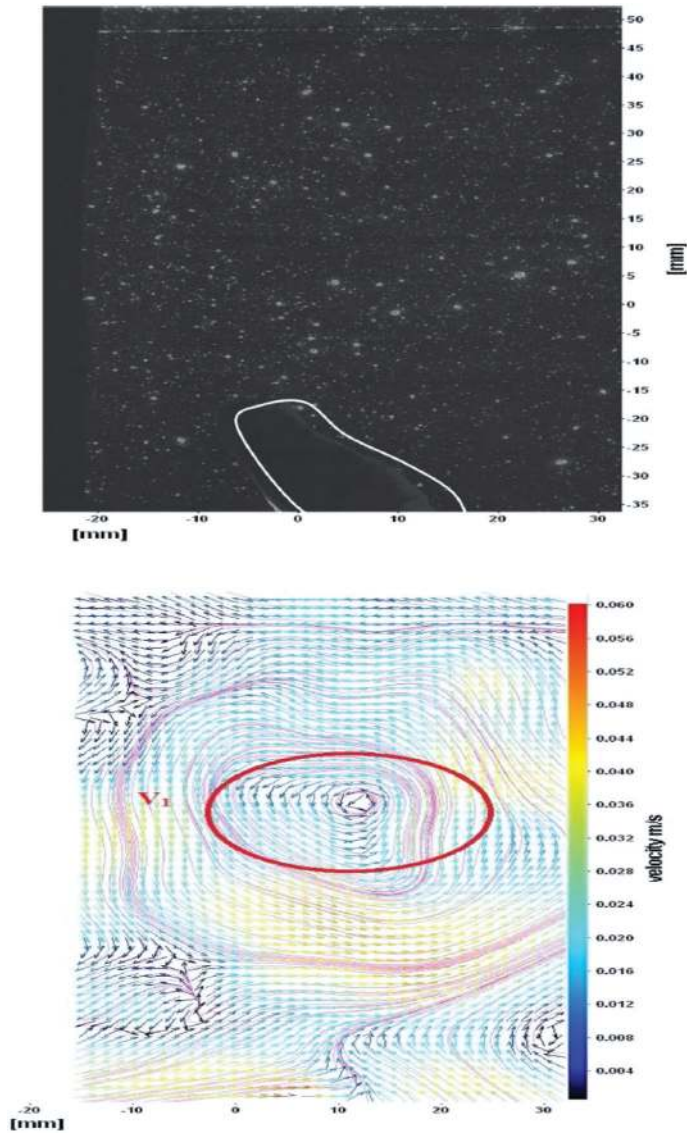
Figure 19.
CCD image and velocity vector field around adipose (upper one) and anal (below one) fins for Δt = 900 ms.

model is tested at different frequencies and constant amplitude and the thrust forces are measured using strain gauges mounted on the caudal fin shaft. The data acquisition system (consists of oscilloscope and amplifier) shown in **Figure 25**. The forward velocity (*V*) of remotely operated surface ship model, fitted with caudal fin, increases until the caudal fin frequency reached about 1.5 Hz and above that the speed of the ship decreases and shown in **Figure 26**. The maximum speed achieved by the vehicle is 0.4 m/s. In self-propulsion tests, a maximum thrust of 8.6 N was recorded at *St* = 0.4 shown in **Figure 27** where the thrust force is plotted against the frequency of flap. In bollard pull, the maximum thrust is found to be 14.8 N at *f* = 1 Hz.

3.5 Experimental study of the remotely operated underwater vehicle with bioinspired caudal fin

The bioinspired robotic fish is shown in **Figure 28** where the body is an axis-symmetric one with a long cylindrical body having a hemispherical nose and conical aft portion, and with a pair of pectoral fins at the forward area and tail (caudal) fin
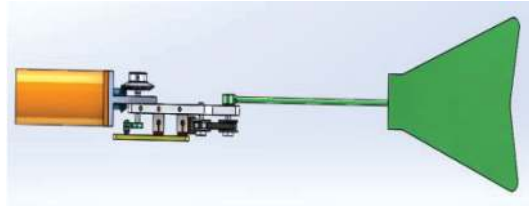
Figure 20.
Consecutive CCD image and velocity vector field around caudal fins stroke at center in YZ plane for Δt = 900 ms.
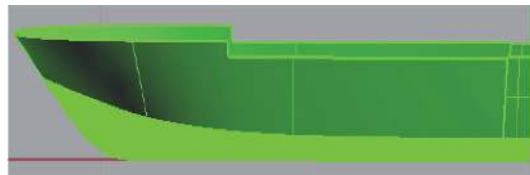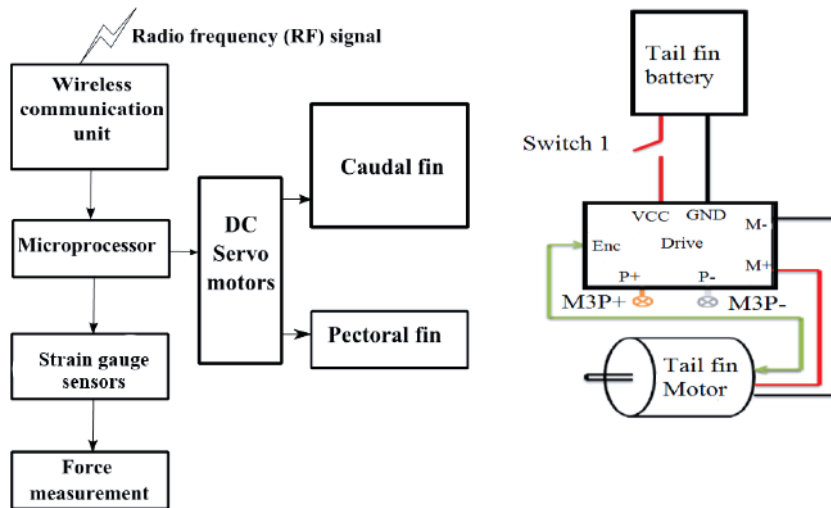

Figure 21.
Remotely operated surface ship model.

at the extreme aft. The principal dimensions of the body are 1.2 m long and 0.16 m diameter. The biomimetic caudal fin fitted at the end of the tail portion of the body acts as the main propulsor for generating thrust. The robotic fish comprises of three individual modules, pectoral fin mechanism, a caudal fin module, and a control system and its battery modules. The hull is made of fiber reinforced plastic (FRP)

Figure 22.
Caudal fin propulsion mechanism.

Figure 23.
Block diagram and caudal fin mechanism connections.

Figure 24.
*Remotely operated surface ship model in the self-propelling mode.*

material of 6 mm thick. The vehicle is propelled by a bioinspired caudal fin in wireless mode. The CFD estimated drag of the underwater vehicle with fins is 48 N and that for the bare hull is 33 N at a speed of 2.5 m/s. As expected, high-pressure regions are seen at the leading edges of pectoral and caudal fins and low-pressure regions are created at the trailing edges of the fins as shown in **Figure 29**. The high-pressure regions are also present in the forward nose of the hull.

3.5.1 Results and discussions

Experiments are conducted to predict the swimming and propulsive behavior of the bioinspired robotic fish in different operating conditions. The tests are
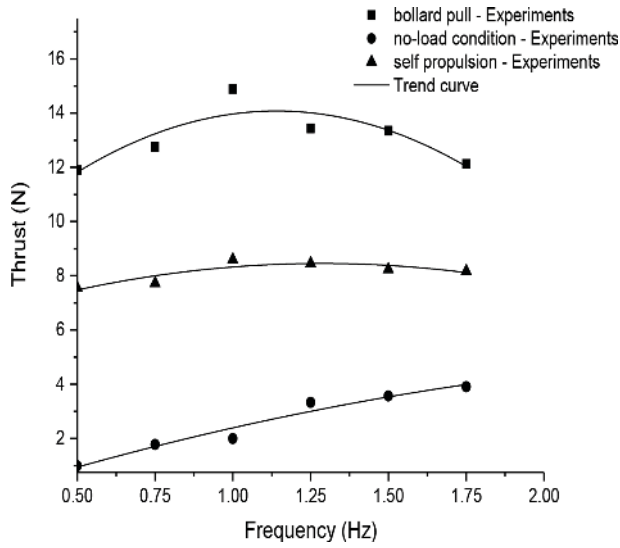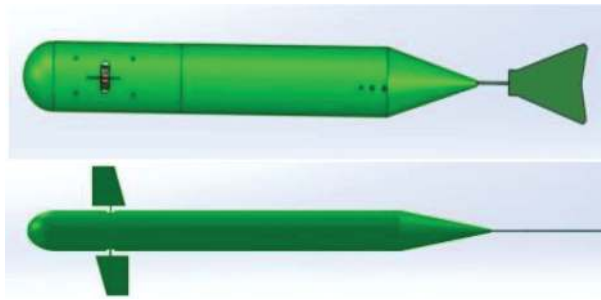
Figure 25.
Data acquisition system.
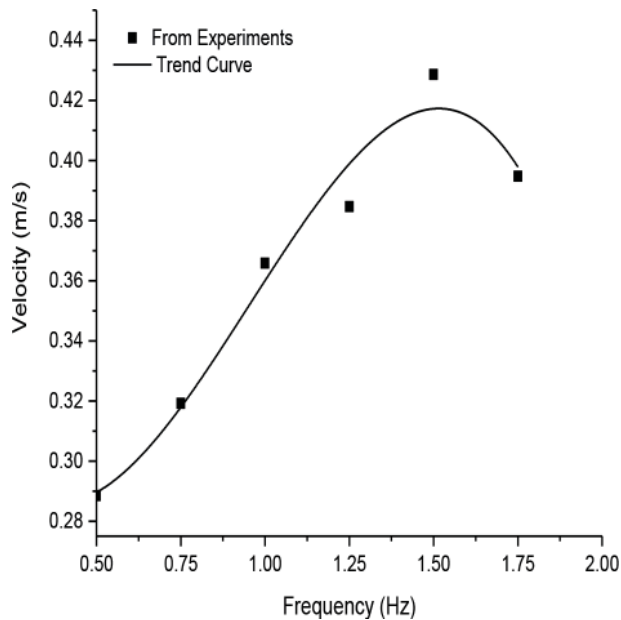
Figure 26.
*Ship model velocity at different oscillation frequencies of the flap.*

conducted in the towing tank and the vehicle swimming velocity and fin developed force is measured. The towing tank dimensions are 82 m long × 3.2 m wide × 3 m depth. The water depth used for all experiments is 2.6 m. The underwater vehicle is propelled by the thrust produced due to the oscillation of caudal fin fitted at the stern part of the vehicle. The swimming velocities at different oscillation frequencies are shown in **Figure 30**. The results show that the fin oscillation generates thrust forces for a range of frequency. At free surface condition, the velocity of 0.53 m/s is achieved at a frequency of 1.5 Hz with an amplitude of 180 mm. In submerged condition, the vehicle achieved a speed of 0.29 m/s. The body attains higher velocity at the surface condition, having less wetted surface area and thus reduced body resistance. In the case of submerged condition, the body resistance is more and hence moved with lesser speed. The thrust force generated by the caudal fin of robotic fish is measured by using strain gauge sensors mounted on the caudal fin shaft. **Figure 31** shows the thrust force developed by the oscillating fin at a different frequency. It is observed that the thrust force increases up to f = 1.0 Hz and then decreases with increase in frequency. The maximum thrust force of about 34.06 N is measured at f = 1.0 Hz in surface condition. A maximum thrust force of 18.6 N is observed in submerged condition

Figure 27.
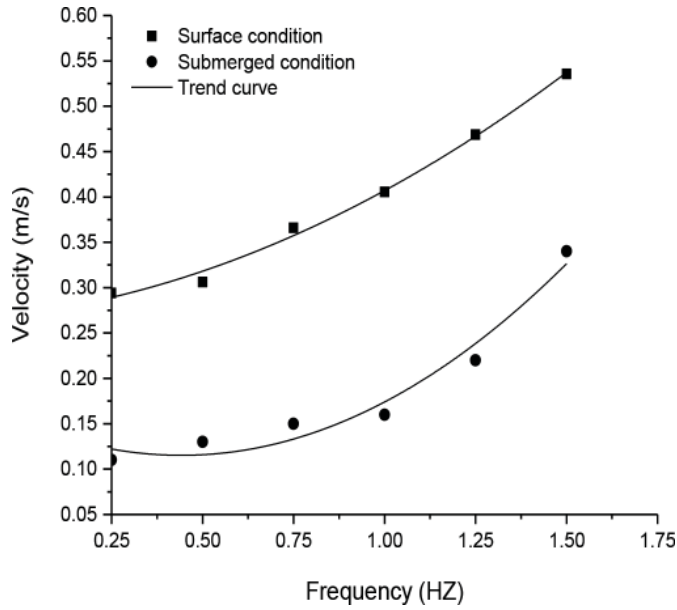*Thrust force developed by the oscillating foil in different ship model operating conditions.*

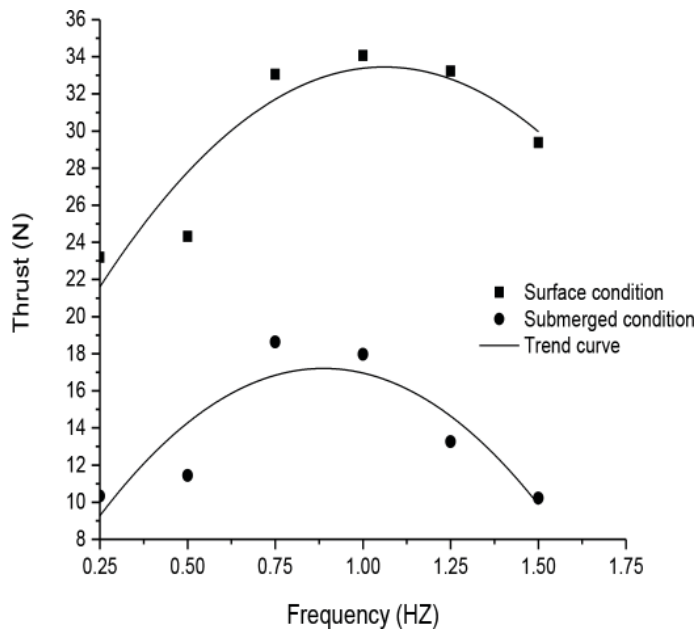**Figure 28.**
Robotic fish with pectoral and caudal fins.
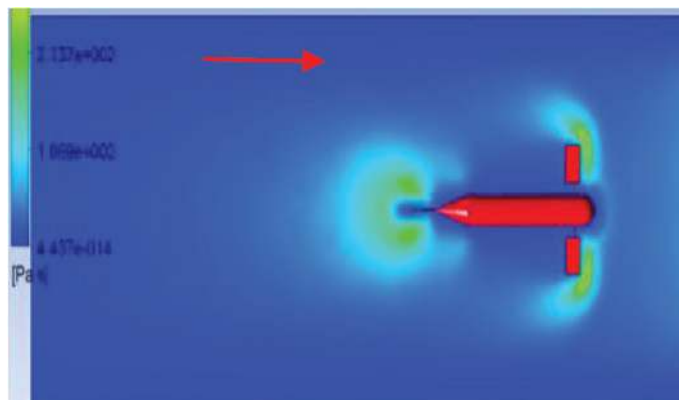
Figure 29.
Flow around the vehicle pectoral and caudal fins (V = 1 m/s).

at f = 0.75 Hz. In submerged condition, caudal fin deformed more due to higher loading and flexibility of fin resulting in reduced performance. As in the surface condition, the thrust produced by the oscillating fin reduced after f = 1.0 Hz.

Figure 30.
Vehicle velocity at different frequencies of the fin at surface piercing and submerged conditions.

Figure 31.
Thrust force developed by the foil at different frequencies at the surface and submerged conditions.

Higher frequency of oscillation results in more flow separation and results in thrust reduction.

4. Summary and conclusions

The design and development of biomimetic robots based on nature locomotion involves multidisciplinary studies such as the biological behavior of fish, flow

visualization around it and its fins during swimming, and numerical and experimental determination of thrust and drag forces. Experimental and numerical studies are carried out to determine the propulsive performance of bioinspired aquatic vehicle fitted with tandem flapping foils. The work has taken shape with the selection of a ship model fitted with a pair of flexible flapping foil at its bottom resembling penguin flippers. The propulsion mechanism developed in Central Workshop (CWS) at IIT Madras is installed at the ship model bottom and then the fins oscillate at different amplitudes and frequencies. Rigid and flexible flapping foils are used in the studies to determine the hydrodynamic forces generated by the flapping foils. In understanding the limitations of potential theory in determining different hydrodynamic parameters, RANSE-based CFD method is used extensively for the numerical studies. A general purpose fluid flow solver FLUENT is used by exploring and exploiting its features to induce dynamic simulations to the fins so as to duplicate the oscillating fin system in the numerical environment. Experimental studies on the ship model, fitted with these penguin type flipper at its bottom, are carried out in the towing tank facility. The thrust generation capability and efficiency of flapping hydrofoils at different parameters (α_0, St, ψ) are studied experimentally and numerically.

In order to understand the natural characteristics of fish swimming, PIV measurements are carried out on a live shark fish to understand and analyze the hydrodynamic behavior of its propulsion using the caudal fin. Sharks exhibit high-performance aquatic locomotion through oscillation of its forked caudal fin. The velocity vector plots show that caudal fins produce reverse von Karman vortex street resulting in an afterward jet formation that gives the propulsive force. This study helped in understanding the flow pattern around the fish and its fins to take the information further to engineering applications. These type of propulsors with improved propulsive characteristics, maneuverability, and creation of less turbulence are inspiring qualities for its adoption in the propulsion of autonomous marine vehicles.

Inspired by the natural aquatic swimming fish, bioinspired remotely operated surface ship and underwater vehicle fitted with caudal fin is studied in detail. The performance of a remotely operated surface ship model propelled by tuna-mimicking caudal fins is evaluated. Design of caudal fin and its control system are carried out. Using the experimental set-up, swimming velocities and thrust forces of a surface ship fitted with the caudal fin in the axial direction are measured at different oscillation frequencies and amplitude of the fin. This information inspired and helped in thinking about the development of a combination of oscillating foil system constituted by the caudal and a pair of pectoral fins to propel underwater vehicles. Numerical studies are used to estimate the drag forces on the body with the bare hull and also the hull fitted with pectoral and caudal fins. The vehicle fitted with caudal fin is studied experimentally at different frequencies and constant amplitude. The thrust force is measured using the strain gauges mounted on the caudal fin connecting rod. The propulsive forces are measured at different oscillation frequencies for the case when the body is surface and below the surface. The vehicle has the ability for better performance, by incorporating pectoral fins also, which will generate additional thrust and also help in the better maneuvering of the vehicle.

Acknowledgements

Conflict of interest

The authors declare that they have no competing interests.

Author details

Naga Praveen Babu Mannam* and P. Krishnankutty
Indian Institute of Technology Madras, Chennai, India

*Address all correspondence to: mpraveenmn@gmail.com

IntechOpen

References

[1] Schouveiler L, Hover FS, Triantafyllou MS. Performance of flapping foil propulsion. Journal of Fluids and Structures. 2005;**20**(7): 949-959

[2] Gottlieb JR, Tangorra JL, Esposito CJ, Lauder GV. A biologically derived pectoral fin for yaw turn maneuvers. Applied Bionics and Biomechanics. 2010;**7**(1):41-55

[3] Lauder GV, Madden PGA, Tangorra JL, Anderson E, Baker TV. Bioinspiration from fish for smart material design and function. Smart Materials and Structures. 2011;**20**(9): 094014

[4] Shinde SY, Arakeri JH. Flexibility in flapping foil suppresses meandering of the induced jet in absence of free stream. Journal of Fluid Mechanics. 2014;**757**:231-250

[5] Lucas KN, Thornycroft PJ, Gemmell BJ, Colin SP, Costello JH, Lauder GV. Effects of non-uniform stiffness on the swimming performance of a passively-flexing, fish-like foil model. Bioinspiration & Biomimetics. 2015; **10**(5):056019

[6] Lua KB, Lu H, Zhang XH, Lim TT, Yeo KS. Aerodynamics of two-dimensional flapping wings in a tandem configuration. Physics of Fluids. 2016; **28**(12):121901

[7] Yang L, Su YM. CFD simulation of flow features and vorticity structures in tuna-like swimming. China Ocean Engineering. 2011;**25**(1):73-82

[8] Hao D, Bao-Wei S, Yong-hui C. Design and prototype development of a 1-DOF flapping-foil and gliding UUV. Journal of Marine Science: Research and Development. 2012;**S10**:001. DOI: 10.4172/2155-9910.S10-001

[9] Ahmed T, Welaya Y, Abdulmotaleb S. Numerical modeling of the hydrodynamic performance of hydrofoils for auxiliary propulsion of ships in regular head-waves. In: Proceedings of the ASME 2017 36th International Conference on Ocean, Offshore and Arctic Engineering OMAE 2017; 25-30 June 2017; Trondheim, Norway; 2017

[10] Mannam NP, Krishnankutty P, Vijayakumaran H, Sunny RC. Experimental and numerical study of penguin mode flapping foil propulsion system for ships. Journal of Bionic Engineering. 2017;**14**(4):770-780

[11] Babu MNP, Mallikarjuna JM, Krishnankutty P. Hydrodynamic study of freely swimming shark fish propulsion for marine vehicles using 2D particle image velocimetry. Robotics and Biomimetics. 2016;**3**(1):3

[12] Mannam NP, Krishnankutty P. Hydrodynamic study of flapping foil propulsion system fitted to the surface and underwater vehicles. Ships and Offshore Structures. 2018:1-9